SIAM J. APPL. MATH.
Vol. 52, No. 4, pp. 1089–1110, August 1992

013

CONTINUUM MODELS OF PLATELET AGGREGATION: FORMULATION AND MECHANICAL PROPERTIES*

AARON L. FOGELSON†

Abstract. Platelet aggregation is an important component of the blood's clotting response, and is associated as well with many forms of cardiovascular disease. A new class of continuum models of platelet aggregation is presented. The models describe interactions among a viscous, incompressible fluid and populations of nonactivated (nonsticky) and activated (sticky) platelets suspended in this fluid. Cohesion between activated platelets can profoundly influence the motion of the suspending fluid. A platelet-activating chemical triggers a platelet's transition from nonactivated to activated status, and induces the secretion of more of the same chemical. Investigation of the mechanical properties of the fluid-platelet system in the absence of new activation shows that platelet cohesion can generate extra pressure and extra viscous and elastic stresses. The last is sufficient to maintain the integrity of an aggregate that is subject to substantial external stress.

Key words. platelet aggregation, continuum models, incompressible viscous flow, convection-diffusion-reaction equations, elasticity, computational fluid dynamics

AMS(MOS) subject classifications. 92, 76, 65

1. Introduction.

This paper is concerned with the development of continuum models of the platelet aggregation process. Platelet aggregation, a major component of the blood-clotting response, involves the clumping together or aggregation of blood platelets along portions of a blood vessel wall in response to injury to the vessel. Platelet aggregates are also a major constituent of the thrombi (blood clots) associated with vascular disease and with the use of blood-contacting prosthetic devices such as vascular grafts and prosthetic cardiac valves. In these settings, undesired aggregate growth can cause severe medical problems. In particular, aggregate formation in the coronary arteries is strongly associated with cardiac ischemia, angina, and myocardial infarction [9], [10]. This paper describes work toward the development of models appropriate for studying aggregation in vessels the size of the coronary arteries or larger.

We begin with a brief sketch of the biology of platelet aggregation. Platelets are cells suspended in the blood. They are present in enormous numbers ($250,000/\text{mm}^3$) yet small volume concentrations (≈ 0.3 percent). Platelets are neutrally buoyant with respect to the blood as a whole. A platelet normally circulates with the blood in a dormant or nonactivated state in which it is not adherent to other platelets or to the blood vessel wall. Stimulation of a nonactivated platelet by certain chemicals triggers the *activation* process in which (1) the platelet's surface membrane is altered so that the platelet becomes "sticky" and capable of cohering with other activated platelets; (2) the platelet secretes into the surrounding fluid chemicals, which can induce activation of other platelets; and (3) the platelet changes morphologically from rigid and discoidal to deformable and spherical, and it extends long thin appendages called pseudopodia. A common hypothesis is that in vivo aggregation is initiated when adhesive platelet-activating tissue embedded in the vessel wall is exposed to the blood because of injury to the vessel [3], [25], [27]. Platelets quickly adhere to this tissue,

* Received by the editors September 10, 1990; accepted for publication (in revised form) September 6, 1991. This work was supported in part by National Science Foundation grant DMS88-03482 and by an Alfred P. Sloan Foundation Fellowship. Part of this work was carried out while the author was a Visiting Member at the Courant Institute of Mathematical Sciences, New York University, New York.

† Department of Mathematics, University of Utah, Salt Lake City, Utah 84112.

and these platelets release activating chemicals into the blood plasma. Other platelets attach to these platelets and to one another and also release activating chemicals. In a short time, platelet aggregates develop at the injured site. While there is no conclusive evidence that the released chemicals potentiate the aggregation in vivo, such a hypothesis is supported by a wide range of in vitro studies. If a sufficiently high concentration of the chemical adenosine diphosphate (ADP), which is one of the released chemicals, is applied to a stirred suspension of platelets, aggregation as well as the secretion of additional ADP by the platelets [15], [27] is observed. Similarly, aggregation and chemical release are induced if the clotting enzyme thrombin is applied to such a suspension [5], [18]. The platelet response to ADP is threshold-like: low doses of exogenous ADP result in reversible aggregation, while doses of sufficiently high concentration lead to "irreversible" aggregation and platelet secretion of ADP. The relative importance of ADP, thrombin, and other activating chemicals to the aggregation process is not clear and is the subject of ongoing experimental investigation [1], [2], [6], [11], [16]. In a qualitative sense, these chemicals act in much the same way. Each chemical serves to carry the activation signal from platelet to platelet by triggering platelet responses, including the secretion of more of the same chemical.

The cohesion of two stimulated platelets is believed to occur through a process in which protein molecules present in the blood plasma bind to receptors on the platelets' surfaces to form intercellular molecular bridges. The leading candidate for the role of bridging molecule is the filamentous protein fibrinogen. There are approximately 50,000 receptors for fibrinogen located on the surface of a platelet, and the activity of these receptors is expressed only when an agonist, such as ADP, acts on the platelet [7], [19]. Cohesion of two platelets also requires contact between them. The long thin pseudopodia extended by platelets upon activation may promote cohesion by increasing the probability of contact. The flexibility of activated platelets permits greater contact between their surface membranes and allows for the formation of tightly packed platelet aggregates [28].

The aggregation events occur in a moving fluid, the blood plasma, or at a fluid-solid interface, the vessel wall, so it is not surprising that a substantial amount of clinical and experimental evidence indicates an important role for the blood's fluid dynamics in controlling the location, rate, and extent of aggregation. Clinical observations suggest that pathological aggregate growth occurs preferentially at sites of relative flow stasis and at sites at which a flow disturbance can be expected, such as near branches, bends, or constrictions of a vessel [10], [12]. Some experimental results suggest that the preferential aggregation associated with the sites of changing vessel geometry may be due to entrapment of platelets and plasma-borne chemicals in eddies near these locations [17]. The rate and extent of platelet adhesion and aggregation on platelet-reactive surfaces in laboratory flow chambers show strong dependence on the flow's shear rate [13], [14], [22]–[24]. Aggregate growth may be limited by high fluid stresses when these stresses are strong enough to break the molecular bridges that attach a new platelet to an aggregate. Similarly, fluid stresses can dislodge portions of an existing aggregate (a process known as embolization) by breaking the connections between platelets within the aggregate [23]. These observations reflect the facts that the growth of aggregates depends in part on fluid-mediated transport of platelets and activating chemicals, and that aggregates grow in an environment in which fluid forces are important. On the other hand, the growth of aggregates projecting into the vessel lumen can markedly influence the flow to the extent that complete vessel occlusion can occur [9]. Thus there is a strong two-way coupling between aggregate growth and

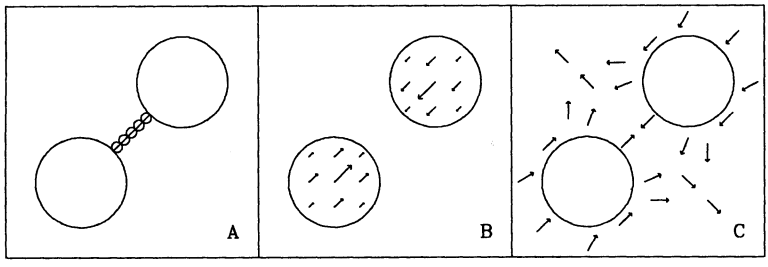

FIG. 1. (A) *In the discrete-platelet model, platelet-platelet cohesion is modelled by an elastic link that joins two platelets.* (B) *Forces generated by the link are spread to the fluid in which the linked platelets are located.* (C) *These fluid forces contribute to the determination of the fluid velocity near the coherent platelets.*

fluid dynamics.

In [8] we present a microscopic scale model of aggregation. That model tracks the motion and behavior of discrete platelets suspended in and interacting with a fluid continuum that represents the nonplatelet portion of the blood. The model is appropriate for studying aggregation in the smallest arteries, which have a diameter of approximately 50μm, but it is not suitable for studying aggregation in vessels the size of the coronary arteries (diameter $\approx$ 1mm) in which the number of platelets is enormous. This paper is concerned with the development of continuum models of aggregation appropriate for such situations. These models differ from the discrete-platelet model of [8] in many ways: most notably in the description of platelets by population density functions and in the inclusion of inertial terms in the equations that describe the fluid dynamics. The formulation of the continuum models was, however, strongly influenced by the modelling of platelet-platelet cohesion in the discrete-platelet model, and so we briefly describe this aspect of that model.

Recall that cohesion between real platelets occurs through the formation of numerous interplatelet molecular bridges. In the discrete-platelet model, this process is modelled by the creation of an elastic link between two activated platelets that come into contact. The links generate forces that resist motions that would otherwise separate the platelets. Recall also that real platelets are neutrally buoyant. We think it reasonable therefore to make the idealization that the mass of a platelet is attributed to the fluid in which the platelet sits and that the platelet itself is massless. As a consequence of the latter, the link forces do not act directly on the platelets, but instead are transmitted to the fluid in the neighborhood of the cohering platelets. These forces drive a fluid motion that keeps the platelets together. (This is illustrated in Fig. 1.) The influence of the platelets on the fluid motion is *solely* through the transmitted forces. The advantage of this modelling approach is that there is no need to keep

track of a moving interface between fluid and aggregates: The aggregates are treated as fluid, but fluid that is characterized by the presence of link-generated contributions to the fluid force density. We note also that, in the discrete-platelet model, an individual platelet that is not interacting directly with another platelet or the vessel wall exerts no force on the surrounding fluid. This is, of course, a simplification. The rationale for this approach is as follows: Platelets constitute only a very small fraction of the blood's volume, most of which ($\approx$ 45 percent) is comprised of red blood cells that are both larger and much more numerous than the platelets. Therefore we expect that the influence of a single platelet on the motion of this concentrated suspension is negligible and that only the cohesive action of aggregated platelets is significant. These ideas are extended to the continuum models that we describe in the next section.

2. Derivation of the models. The continuum models are based upon the interactions among a viscous, incompressible fluid; populations of nonactivated and activated platelets; a distribution of interplatelet links; and an interplatelet signalling chemical. For simplicity, we generally refer to this chemical as ADP. As indicated earlier, there are several activating chemicals that act in a qualitatively similar fashion, and, in the current qualitative models, it is unnecessary to distinguish between them. The current formulations of the model do not include interactions between platelets and a vessel wall. That is the subject of future work.

As in the discrete platelet aggregation model described above, we treat the fluid and platelet mixture as a composite. We attribute the mass and volume of each (neutrally buoyant) platelet to the fluid in which it sits. The platelet moves at the local fluid velocity $\mathbf{u}(\mathbf{x}, t)$, which therefore may also be interpreted as the velocity of the mixture. (Some platelets also have a random component to their motion as we explain below.) An activated platelet is distinguished from other fluid particles in that its cohesion with other activated platelets leads to the generation of cohesion forces that can strongly influence the fluid's motion. The treatment of cohesion and the nature of the forces it can generate are important components of the modelling and analysis we present below.

In the macroscopic setting of the continuum models, the distance between the centers of cohering platelets is much smaller than the macroscopic length scale as measured, for example, by the vessel diameter. Thus a small parameter ϵ appears in the models; it is the ratio of a typical link distance (roughly a platelet diameter) to the macroscopic length scale. We are interested in the situation where it is appropriate to let $\epsilon \to 0$, and the model that is presented below consists of the zeroth-order terms in an expansion in powers of ϵ.

The unknown functions in the model are as follows:

(a)	$\mathbf{u}(\mathbf{x}, t)$:	the fluid velocity field,
(b)	$p(\mathbf{x}, t)$:	the pressure,
(c)	$\epsilon^{-3}\phi_n(\mathbf{x}, t)$:	the concentration of nonactivated platelets,
(d)	$\epsilon^{-3}\phi_a(\mathbf{x}, t)$:	the concentration of activated platelets,
(e)	$c(\mathbf{x}, t)$:	the concentration of signaling chemical ADP, and
(f)	$P(\mathbf{x}, \epsilon^{-1}\mathbf{r}, t)$:	the expected number of elastic links that join a given activated platelet at $\mathbf{x}$ to a given activated platelet at $\mathbf{x} + \mathbf{r}$.

In these expressions, $\mathbf{x}$ is a spatial location and t denotes time. The scaling in definitions (c) and (d) is used because, in a fixed macroscopic volume of aggregate in which

platelets are spaced approximately a distance ϵ from one another, the total number of platelets scales as ϵ^{-3}. We expect the function P, defined in (f), to be nearly zero for $|\mathbf{r}|$ much larger than ϵ.

In the description that follows, it is often useful to make the change of variable $\mathbf{v} = \epsilon^{-1}\mathbf{r}$. Thus $\mathbf{v}$ is the scaled link vector, and $P(\mathbf{x}, \mathbf{v}, t)$ is the expected number of elastic links that join a given activated platelet at $\mathbf{x}$ to a given activated platelet at $\mathbf{x} + \epsilon\mathbf{v}$.

The following are the equations of one form of the model:

$$\rho(\mathbf{u}_t + \mathbf{u} \cdot \nabla\mathbf{u}) = -\nabla p + \mu\Delta\mathbf{u} + \mathbf{f}^g + \mathbf{f}^p, \tag{1}$$

$$\nabla \cdot \mathbf{u} = 0, \tag{2}$$

$$\frac{\partial \phi_n}{\partial t} + \mathbf{u} \cdot \nabla\phi_n = D_n\Delta\phi_n - R(c)\phi_n, \tag{3}$$

$$\frac{\partial \phi_a}{\partial t} + \mathbf{u} \cdot \nabla\phi_a = R(c)\phi_n, \tag{4}$$

$$c_t + \mathbf{u} \cdot \nabla c = D_c\Delta c + AR(c)\phi_n, \tag{5}$$

$$(\phi_a^2 P)_t + \mathbf{u} \cdot \nabla_x(\phi_a^2 P) + (\mathbf{v} \cdot \nabla\mathbf{u}) \cdot \nabla_v(\phi_a^2 P) = \alpha\phi_a^2 - \beta\phi_a^2 P, \tag{6}$$

$$\mathbf{f}^p = \frac{1}{2}\int \mathbf{v} \cdot \nabla_x\{\phi_a(\mathbf{x}, t)^2 P(\mathbf{x}, \mathbf{v}, t)\}S(|\mathbf{v}|)\mathbf{v}\,d\mathbf{v}. \tag{7}$$

Equations (1) and (2) are the Navier–Stokes equations that describe the dynamics of a viscous incompressible fluid [4]. In these equations, ρ is the fluid's mass density, and μ is its viscosity. Both of these are assumed to be constant. Equation (1) contains two force density terms, one of which, $\mathbf{f}^g$, corresponds to a applied body force such as might drive a background flow (see the examples in §3.4), and the other of which, $\mathbf{f}^p$, corresponds to forces generated by the platelet-platelet links. We call $\mathbf{f}^p$ the cohesion-force density.

Equation (3) expresses the assumption that nonactivated platelets are transported by convection with velocity $\mathbf{u}$ and diffusion with diffusion coefficient D_n, and are converted to activated platelets at a rate $R(c)\phi_n$, which depends on the concentration c of ADP. Equation (4) describes the transport of activated platelets by convection and their creation by the activation of nonactivated platelets. Diffusive transport of platelets is included in the model to reflect the experimental observation that, in flowing blood, platelets have a random component to their motion two orders of magnitude larger than that which would result from Brownian motion [20]. The enhanced diffusivity is correlated with the presence of the larger and more numerous red blood cells, which make up 45 percent of the volume of normal blood [12], [26]. It is thought that shear-induced tumbling and colliding of the nonspherical red blood cells causes a local mixing of the blood, thus imparting to the platelets a diffusion-like motion [21], [26]. It is reasonable to expect that the influence of these local

disturbances on a particle's motion decreases as the size of the particle increases. We also expect that the influence of these disturbances is small for all particles in a region where the density of aggregates is high. Thus the diffusivity of individual nonactivated platelets should be greater than that of aggregated activated platelets, and both diffusivities should decrease with increasing aggregate density. For simplicity, we assume for now that nonactivated platelets have a positive constant diffusivity, while activated platelets have zero diffusivity. The influence of variable diffusion will be considered in later studies.

Equation (5) states that the signaling chemical (ADP) is transported by convection and diffusion and is created when nonactivated platelets are activated. The rate of creation is the amount A of ADP (assumed constant) that a single platelet secretes upon activation multiplied by the rate $R(c)\phi_n$ at which nonactivated platelets are activated.

The origins of (6) and (7) require more detailed explanation. Equation (6) is derived from the integral conservation law

$$
\begin{aligned}
&\frac{d}{dt}\int_{\Omega_x(t)}\int_{\Omega_y(t)} \epsilon^{-3}\phi_a(\mathbf{x},t)\epsilon^{-3}\phi_a(\mathbf{y},t)P(\mathbf{x},\epsilon^{-1}(\mathbf{y}-\mathbf{x}),t)\,d\mathbf{y}d\mathbf{x}\\
&= \int_{\Omega_x(t)}\int_{\Omega_y(t)} \alpha(|\epsilon^{-1}(\mathbf{y}-\mathbf{x})|)\epsilon^{-3}\phi_a(\mathbf{x},t)\epsilon^{-3}\phi_a(\mathbf{y},t)\,d\mathbf{y}d\mathbf{x}\\
&\quad - \int_{\Omega_x(t)}\int_{\Omega_y(t)} \beta(|\epsilon^{-1}(\mathbf{y}-\mathbf{x})|)\epsilon^{-3}\phi_a(\mathbf{x},t)\epsilon^{-3}\phi_a(\mathbf{y},t)P(\mathbf{x},\epsilon^{-1}(\mathbf{y}-\mathbf{x}),t)\,d\mathbf{y}d\mathbf{x}.
\end{aligned}
\tag{8}
$$

In this equation, $\Omega_x(t)$ and $\Omega_y(t)$ are arbitrary material volumes. The equation expresses our assumption that the total number of links between activated platelets in region $\Omega_x(t)$ and activated platelets in region $\Omega_y(t)$ increases at a rate equal to the rate of creation of new links less the rate of breaking of existing links. The link-formation rate function $\alpha(|\mathbf{v}|) = \alpha(|\epsilon^{-1}(\mathbf{y}-\mathbf{x})|)$ is assumed to have support in an interval of length $O(1)$, so that links may be formed only between activated platelets that are near one another. In this paper, we assume that the link-breaking rate function $\beta(|\mathbf{v}|)$ is a constant β_0. In (8) we ignore saturation in the link-creation term; that is, we ignore the fact that there is a limit to the number of links that a given platelet can form. Our rationale for this is that we expect the actual number of links formed by a platelet to be much less than the maximum possible number of links (n), as measured by the number of binding sites on an activated platelet for the intercellular bridging molecule. To account for possible saturation, the link-formation term would have to be specified to ensure that the constraint $\int_V P(\mathbf{x},\mathbf{v},t)d\mathbf{v} \le n$ was satisfied. One way to do this would be to assume that links between platelets in $\Omega_x(t)$ and $\Omega_y(t)$ form at a rate

$$
\int_{\Omega_x(t)}\int_{\Omega_y(t)} \epsilon^{-3}\phi_a(\mathbf{x},t)\epsilon^{-3}\phi_a(\mathbf{y},t)\tilde{\alpha}(|\epsilon^{-1}(\mathbf{y}-\mathbf{x})|)\left\{n - \int_V P(\mathbf{x},\mathbf{v},t)d\mathbf{v}\right\}\left\{n - \int_V P(\mathbf{x},\mathbf{v},t)d\mathbf{v}\right\} d\mathbf{y}d\mathbf{x}.
$$

In using the term in (8), we assume that $\int_V P(\mathbf{x},\mathbf{v},t)d\mathbf{v} \ll n$, and set $\alpha(|\epsilon^{-1}(\mathbf{y}-\mathbf{x})|) = n^2\,\tilde{\alpha}(|\epsilon^{-1}(\mathbf{y}-\mathbf{x})|)$.

To derive (6) from (8), we make the change of variables $\mathbf{y}-\mathbf{x} = \epsilon\mathbf{v}$, expand the resulting function $\phi_a(\mathbf{x}+\epsilon\mathbf{v},t)$ in a Taylor series about $\mathbf{x}$, evaluate the total time derivative on the left-hand side, and retain only the zeroth-order terms in ϵ.

Details of the derivation are given in Appendix A. The unusual $(\mathbf{v}\cdot\nabla\mathbf{u})\cdot\nabla_v(\phi_a^2 P)$ term in (6) arises because of the difference between $\mathbf{u}$ at $\mathbf{x}$ and $\mathbf{x}+\epsilon\mathbf{v}$. This term describes convection of $(\phi_a^2 P)$ in $\mathbf{v}$-space at "velocity" $\mathbf{v}\cdot\nabla\mathbf{u}$. It is a consequence of the incompressibility of $\mathbf{u}$ that the divergence of $\mathbf{v}\cdot\nabla\mathbf{u}$ is zero.

The force density expression given in (7) is derived from the more fundamental expression

$$\mathbf{f}^p(\mathbf{x},t)=\epsilon^{-3}\phi_a(\mathbf{x},t)\int P(\mathbf{x},\epsilon^{-1}\mathbf{r},t)\epsilon^{-3}\phi_a(\mathbf{x}+\mathbf{r},t)\mathbf{F}(\epsilon^{-1}\mathbf{r})d\mathbf{r}. \tag{9}$$

The integral here is over all $\mathbf{r}$. The function $\mathbf{F}(\epsilon^{-1}\mathbf{r})$ is the force associated with a single link whose link vector is $\mathbf{r}$. Equation (9) is the statement that the force on a small region of fluid around the point $\mathbf{x}$ due to platelet-platelet cohesion is the sum of the individual link forces for links that join activated platelets within this small region to other activated platelets. We assume that the function $\mathbf{F}(\epsilon^{-1}\mathbf{r})$ scales as ϵ^2; i.e., we assume that $\mathbf{F}(\epsilon^{-1}\mathbf{r}) = \epsilon^2 S(|\epsilon^{-1}\mathbf{r}|)\epsilon^{-1}\mathbf{r}$. The rationale for this assumption is that the number of links crossing a given macroscopic surface scales as ϵ^{-2}, and so to preserve the material properties (e.g., stiffness) of the aggregates as $\epsilon\to 0$, the force per link should scale as ϵ^2. This is also the only scaling that gives a finite expression for $\mathbf{f}^p$. Using this scaling for $\mathbf{F}$ in (9), making the change of variables $\mathbf{r}=\epsilon\mathbf{v}$ as before, expanding the function $\phi_a(\mathbf{x}+\epsilon\mathbf{v},t)$ in a Taylor series about $\mathbf{x}$, and using the fact $P(\mathbf{x},-\mathbf{v},t)=P(\mathbf{x}-\epsilon\mathbf{v},\mathbf{v},t)$, we obtain (7) as the leading (nonvanishing) term. (See Appendix B for details.) The relation $P(\mathbf{x},-\mathbf{v},t)=P(\mathbf{x}-\epsilon\mathbf{v},\mathbf{v},t)$ holds because each of these expressions describes the expected number of links that join a platelet at $\mathbf{x}$ and one at $\mathbf{x}-\epsilon\mathbf{v}$.

The cohesion-force density $\mathbf{f}^p$ may also be expressed as the divergence of the cohesion-stress tensor $\underline{\underline{\sigma^p}}(\mathbf{x},t)$ defined by the equation

$$\underline{\underline{\sigma^p}}(\mathbf{x},t)=\frac{1}{2}\phi_a(\mathbf{x},t)^2\int P(\mathbf{x},\mathbf{v},t)S(|\mathbf{v}|)\mathbf{v}\mathbf{v}^T d\mathbf{v}. \tag{10}$$

3. Mechanical properties of the fluid-link system. In the remainder of this paper, we examine the properties of a major subsystem of the above model, namely, that comprised of the fluid, a population of activated platelets, and a population of interplatelet links. No new activation is permitted in this investigation, and activation chemistry is ignored. We are interested in the nature of the forces or stresses generated by the interplatelet links and, in particular, whether they are capable of maintaining the integrity of a platelet aggregate in the face of substantial external stresses.

3.1. Cohesion-force density in steady state with no flow. We consider the model equations (1)–(7) in a steady-state situation in which there is no flow ($\mathbf{u}=0$). For this situation, the link distribution is isotropic and is given by

$$P(\mathbf{v})=\frac{\alpha(|\mathbf{v}|)}{\beta_0}, \tag{11}$$

and the cohesion-force density (7) reduces to

$$\mathbf{f}^p(\mathbf{x})=\left(\int\frac{\alpha(|\mathbf{v}|)S(|\mathbf{v}|)}{2\beta_0}\mathbf{v}\mathbf{v}^T d\mathbf{v}\right)\nabla_x(\phi_a(\mathbf{x},t)^2). \tag{12}$$

The expression in parentheses is a matrix. All the off-diagonal terms involve an integrand that is odd in some component of $\mathbf{v}$, and so these terms vanish. The

diagonal terms are all equal, and so the integral is a constant multiple of the identity matrix. In this case, therefore, the cohesion-force density $\mathbf{f}^p$ is a gradient, and so it is equivalent to an additional pressure term in the Navier–Stokes equations (1). The sign of the additional pressure depends on the link stiffness function $S(|\mathbf{v}|)$. If each link behaves like a linear spring with resting length 0, $S(|\mathbf{v}|) = K_0$, where $K_0 > 0$ is constant and $\mathbf{f}^p$ is the gradient of a positive function. Since the pressure term and the cohesion-force density term have opposite signs in (1), the extra pressure term corresponds to a *negative* pressure. To see that this is reasonable, consider a radially symmetric distribution of activated platelets $\phi_a(\mathbf{x}) = \phi_0(|\mathbf{x}|)$ with $\phi_0' < 0$ for $|\mathbf{x}| > 0$. Then, $\nabla_x(\phi_a(\mathbf{x},t)^2)$, and therefore $\mathbf{f}^p$, everywhere point toward the origin. For each platelet along a circle $|\mathbf{x}| = r$, there are more links to platelets inside the circle than to those outside. The result is "suction," which tries to draw the platelets (and fluid) on $|\mathbf{x}| = r$ toward the origin. Radially symmetric flow toward the origin is not possible for an incompressible fluid. The mechanism for preventing flow is a change in the fluid pressure to balance $\mathbf{f}^p$. Also in the nonradially symmetric case, the fluid pressure balances $\mathbf{f}^p$, and no flow occurs.

3.2. Flow between parallel plates. In the presence of flow, the links do more than generate extra pressure. We consider the model's equations in the domain $D = \{\mathbf{x} : 0 \le x_2 \le 1\}$, and we make the assumption that no new activation occurs. Since we may ignore ϕ_n and c, the relevant equations are as follows:

$$\rho(\mathbf{u}_t + \mathbf{u}\cdot\nabla\mathbf{u}) = -\nabla p + \mu\Delta\mathbf{u} + \mathbf{f}^p, \tag{13}$$

$$\nabla\cdot\mathbf{u} = 0, \tag{14}$$

$$\frac{\partial\phi_a}{\partial t} + \mathbf{u}\cdot\nabla\phi_a = 0, \tag{15}$$

$$P_t + \mathbf{u}\cdot\nabla_x P + (\mathbf{v}\cdot\nabla\mathbf{u})\cdot\nabla_v P = \alpha(\mathbf{v}) - \beta_0 P, \tag{16}$$

$$\mathbf{f}^p = \frac{1}{2}\int \mathbf{v}\cdot\nabla_x(\phi_a^2 P)S(|\mathbf{v}|)\mathbf{v}\,d\mathbf{v}. \tag{17}$$

Equation (16) is obtained from (6) by use of (15). The boundary condition imposed on $\mathbf{u}$ at $x_2 = 0$ and $x_2 = 1$ is the no-slip condition. No boundary conditions are necessary for ϕ_a or P. We seek a steady-state solution with $\mathbf{u} = (x_2/\tau_0, 0, 0)$ and with the other unknowns p, ϕ_a, and P, independent of $\mathbf{x}$. Here τ_0 is a characteristic time for the flow between two flat plates; a stationary one at $x_2 = 0$ and one moving with speed τ_0^{-1} at $x_2 = 1$. In the absence of the cohesion-force density, this linear flow would be the solution to (13) and (14). We assume that this flow is maintained in the presence of the links and ask what additional stresses, in particular, shear stresses, are generated by the links.

With the assumptions we have made, we find that $p = p_0$ (constant), $\phi_a = \phi_0$ (constant), and $\mathbf{f}^p = 0$. We also find that (16) reduces to

$$\tau_0^{-1} v_2 \frac{\partial}{\partial v_1} P = \alpha(|\mathbf{v}|) - \beta_0 P, \tag{18}$$

and that, from (10), the cohesion stress tensor has constant elements

$$\sigma^p_{jk} = \frac{1}{2}\phi_0^2 \int P(\mathbf{v}) S(|\mathbf{v}|) v_j v_k d\mathbf{v}. \tag{19}$$

We seek a function $P(\mathbf{v})$ that satisfies (18) and that also satisfies the constraint

$$P(-\mathbf{v}) = P(\mathbf{v}). \tag{20}$$

This constraint is a special case, for the situation P independent of $\mathbf{x}$ and t, of the relation $P(\mathbf{x}, -\mathbf{v}, t) = P(\mathbf{x} - \epsilon\mathbf{v}, \mathbf{v}, t)$ discussed earlier. For $v_2 = 0$, (18) has solution

$$P(v_1, 0, v_3) = \alpha(|\mathbf{v}|)/\beta_0. \tag{21}$$

Since (18) is invariant under reflection of $\mathbf{v}$ through the origin, if $P_+(\mathbf{v})$ is a solution of this equation for $v_2 > 0$ and for all v_1 and v_3, then $P_+(-\mathbf{v})$ is a solution for $v_2 < 0$. For $v_2 > 0$, (18) may be integrated directly. Let $\gamma(|\mathbf{v}|) = \alpha(|\mathbf{v}|)/\beta_0$. Then

$$P(\mathbf{v}) = \frac{\beta_0 \tau_0}{v_2} \int_{-\infty}^{v_1} \gamma(\sqrt{s^2 + v_2^2 + v_3^2}) e^{\beta_0 \tau_0 (s - v_1)/v_2} ds. \tag{22}$$

We note that (22) is consistent with (21) as $v_2 \to 0$. We consider the special case in which links form only when the interplatelet separation is sufficiently small and then do so at a constant rate α_0

$$\alpha(|\mathbf{v}|) = \begin{cases} \alpha_0 & \text{if } |\mathbf{v}| < r_0, \\ 0 & \text{if } |\mathbf{v}| > r_0. \end{cases} \tag{23}$$

We let $\gamma_0 = \alpha_0/\beta_0$ and $b = {r_0}^2 - {v_2}^2 - {v_3}^2$. Then (22) yields

$$P(\mathbf{v}) = \begin{cases} 0 & \text{if } b < 0, \\ \gamma_0 \left\{1 - e^{-(\beta_0\tau_0/v_2)(v_1 + \sqrt{b})}\right\} & \text{if } b > 0 \text{ and } |v_1| < \sqrt{b}, \\ 0 & \text{if } b > 0 \text{ and } v_1 < -\sqrt{b}, \\ \gamma_0 e^{-(\beta_0\tau_0/v_2)v_1}\, 2 \sinh\{(\beta_0\tau_0/v_2)\sqrt{b}\} & \text{if } b > 0 \text{ and } v_1 > \sqrt{b}. \end{cases} \tag{24}$$

The shear flow skews the distribution of interplatelet links as is illustrated in Fig. 2. Use of the formula for P given in (24), along with specification of the link stiffness function $S(|\mathbf{v}|)$, suffices to determine the cohesion-stress tensor from (19). We assume that $S(|\mathbf{v}|) = K_0$; that is, we assume that each link behaves as a linear spring with zero resting length. Then we find that

$$\sigma^p_{12} = \left(\frac{2\pi r_0^5}{15}\right) K_0 \phi_0^2 \left(\frac{\alpha_0}{\beta_0}\right) \frac{1}{\tau_0 \beta_0}, \tag{25}$$

$$\sigma^p_{13} = \sigma^p_{23} = 0, \tag{26}$$

$$\sigma^p_{11} = \left(\frac{2\pi r_0^5}{15}\right) K_0 \phi_0^2 \left(\frac{\alpha_0}{\beta_0}\right) \left\{1 + \frac{2}{\tau_0 \beta_0}\right\}, \tag{27}$$

$$\sigma^p_{22} = \sigma^p_{33} = \left(\frac{2\pi r_0^5}{15}\right) K_0 \phi_0^2 \left(\frac{\alpha_0}{\beta_0}\right). \tag{28}$$

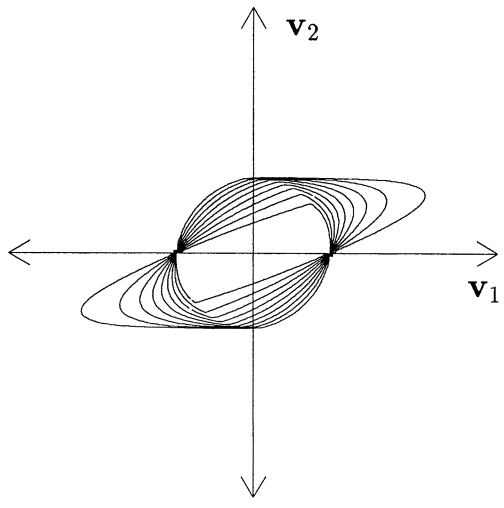

FIG. 2. *Contour lines of the function $P(v_1, v_2, v_3)$ in a steady-state shear flow. The figure depicts the plane $v_3 = 0$. The distribution of links is skewed in the direction of the shear.*

In particular, we see from (25) that the total shear stress on the fluid is

$$\sigma_{12} = \left[\mu + \left(\frac{2\pi r_0^5}{15}\right) K_0 \phi_0^2 \left(\frac{\alpha_0}{\beta_0}\right) \frac{1}{\beta_0}\right] \tau_0^{-1}, \tag{29}$$

so that, in this steady-state situation, the interplatelet links augment the fluid viscosity μ by an amount proportional to the product of the spring constant, the square of the concentration of activated platelets, and the ratio of link formation to link-breaking rates.

3.3. Linear stability analysis of the fluid-link system. To see whether the fluid-link system has *elastic* properties and to explore the nature of these properties, we perform a linear stability analysis of the fluid dynamics equations coupled to those for transport of activated platelets and links. We assume that no new activation occurs and consider again (13)–(17). We again let $\gamma(|\mathbf{v}|) = \alpha(|\mathbf{v}|)/\beta_0$. Then the equations have a steady-state, $\mathbf{x}$-independent solution $\mathbf{u} = \mathbf{u}_0 =$ constant, $p = p_0 =$ constant, $\phi_a = \phi_0 =$ constant, $P = P_0 = \gamma(|\mathbf{v}|)$, $\mathbf{f}^p = \mathbf{f}_0^p = 0$. Without loss of generality, we may set $\mathbf{u}_0 = 0$ since nonzero $\mathbf{u}_0$ just results in uniform translation of the entire solution. We consider a perturbation of this special solution of the following form:

$$\mathbf{u} = \delta \mathbf{u}_1(\mathbf{x}, t), \tag{30}$$

$$p = p_0 + \delta p_1(\mathbf{x}, t), \tag{31}$$

$$\phi_a = \phi_0 + \delta \phi_1(\mathbf{x}, t), \tag{32}$$

$$P = \gamma(|\mathbf{v}|) + \delta P_1(\mathbf{x}, \mathbf{v}, t). \tag{33}$$

From (13)–(17), we obtain the following linearized equations for $\mathbf{u}_1$, p_1, ϕ_1, and P_1:

(34)
$$\rho \mathbf{u}_{1,t} = -\nabla p_1 + \mu \Delta \mathbf{u}_1 + \int \mathbf{v} \cdot \left\{ \frac{1}{2}\phi_0^2 \nabla P_1(\mathbf{x}, \mathbf{v}, t) + \phi_0 \gamma(|\mathbf{v}|) \nabla \phi_1 \right\} S(|\mathbf{v}|) \mathbf{v} d\mathbf{v},$$

(35)
$$\nabla \cdot \mathbf{u}_1 = 0,$$

(36)
$$\phi_{1,t} = 0,$$

(37)
$$P_{1,t} + \frac{\gamma'(|\mathbf{v}|)}{|\mathbf{v}|} (\mathbf{v} \cdot \nabla \mathbf{u}_1) \cdot \mathbf{v} = -\beta_0 P_1.$$

In deriving these equations, we use the equation $P_0(\mathbf{v}) = \gamma(|\mathbf{v}|)$ to write $(\mathbf{v} \cdot \nabla \mathbf{u}) \cdot \nabla_{\mathbf{v}} P_0 = (\gamma'(|\mathbf{v}|)/|\mathbf{v}|)(\mathbf{v} \cdot \nabla \mathbf{u}_1) \cdot \mathbf{v}$. We also substitute the cohesion-force expression into the momentum equation (13). We now make a specific assumption about the form of the perturbation. Let

(38)
$$\mathbf{u}_1 = \hat{\mathbf{u}} e^{i(\omega t - \mathbf{k} \cdot \mathbf{x})},$$

(39)
$$p_1 = \hat{p} e^{i(\omega t - \mathbf{k} \cdot \mathbf{x})},$$

(40)
$$\phi_1 = 0,$$

(41)
$$P_1 = \hat{P}(\mathbf{v}) e^{i(\omega t - \mathbf{k} \cdot \mathbf{x})}.$$

Here $\mathbf{k} \in \mathbb{R}^3$, and $\omega \in \mathbb{C}$. For each $\mathbf{k}$, the quantities $\hat{\mathbf{u}}$ and $\hat{p}$ are complex constants, and $\hat{P}$ is a complex-valued function of $\mathbf{v}$. We note that if we assume that $\phi_1 = \hat{\phi} e^{i(\omega t - \mathbf{k} \cdot \mathbf{x})}$, then (36) requires that $\hat{\phi} = 0$ or $\omega = 0$. The latter is not interesting. By substituting expressions (38)–(41) into (34)–(37), we obtain the following system:

(42)
$$i\rho\omega \hat{\mathbf{u}} = i\mathbf{k}\hat{p} - \mu |\mathbf{k}|^2 \hat{\mathbf{u}} - i\frac{1}{2}\phi_0^2 \int (\mathbf{v} \cdot \mathbf{k}) \hat{P}(\mathbf{v}) S(|\mathbf{v}|) \mathbf{v} d\mathbf{v},$$

(43)
$$\mathbf{k} \cdot \hat{\mathbf{u}} = 0,$$

(44)
$$i\omega \hat{P} - i\frac{\gamma'(|\mathbf{v}|)}{|\mathbf{v}|} (\mathbf{v} \cdot \mathbf{k})(\mathbf{v} \cdot \hat{\mathbf{u}}) = -\beta_0 \hat{P}.$$

If $i\omega + \beta_0 = 0$, then $\hat{P}$ is arbitrary, $\hat{\mathbf{u}} = 0$, and the perturbation decays with time constant β_0. For the remainder of this section, we assume that $i\omega + \beta_0 \neq 0$. We solve (44) for $\hat{P}$ in terms of $\hat{\mathbf{u}}$ and substitute this into (42) to obtain an equation that involves $\hat{\mathbf{u}}$ and $\hat{p}$. We take the dot product of this equation with $\mathbf{k}$ and use (43) to obtain an expression for $\hat{p}$ in terms of $\hat{\mathbf{u}}$. Substituting this back into the equation for $\hat{\mathbf{u}}$ and $\hat{p}$, we obtain that

(45)
$$i\rho\omega \hat{\mathbf{u}} + \mu |\mathbf{k}|^2 \hat{\mathbf{u}} = \frac{1}{2}\phi_0^2 \int \left[\mathbf{v} - \frac{\mathbf{v} \cdot \mathbf{k}}{|\mathbf{k}|^2} \mathbf{k} \right] \frac{(\mathbf{v} \cdot \mathbf{k})^2 (\mathbf{v} \cdot \hat{\mathbf{u}})}{\beta_0 + i\omega} \frac{\gamma'(|\mathbf{v}|)}{|\mathbf{v}|} S(|\mathbf{v}|) d\mathbf{v}.$$

The right-hand side of (45) includes all of the influence of the interplatelet links in the linearized system. Without these links, (45) implies that $\omega = i(\mu/\rho)|\mathbf{k}|^2$, and so the fluid viscosity causes the perturbation to decay. As we will see, when the links are present, more interesting behavior is possible. Consider the integral

$$\mathbf{I} = \int \left[\mathbf{v} - \frac{\mathbf{v}\cdot\mathbf{k}}{|\mathbf{k}|^2}\mathbf{k}\right](\mathbf{v}\cdot\mathbf{k})^2(\mathbf{v}\cdot\hat{\mathbf{u}})\frac{\gamma'(|\mathbf{v}|)}{|\mathbf{v}|}S(|\mathbf{v}|)d\mathbf{v}, \tag{46}$$

which appears in (45). To simplify this integral, we introduce a Cartesian coordinate system with axes in the directions $\mathbf{w}_0$, $\mathbf{w}_1$, and $\mathbf{w}_2$, where $\mathbf{w}_i$, $i = 0, 1, 2$ is a unit vector and $\mathbf{w}_0 = \mathbf{k}/|\mathbf{k}|$. We make the change of variables $\mathbf{v} = w_0\mathbf{w}_0 + w_1\mathbf{w}_1 + w_2\mathbf{w}_2$ and use the fact that $\hat{\mathbf{u}}\cdot\mathbf{w}_0 = 0$ (see (43)) to obtain that

$$\mathbf{I} = M|\mathbf{k}|^2\hat{\mathbf{u}}, \tag{47}$$

where the important quantity M is defined by

$$M = \int \left[w_0^2 w_j^2 \frac{\gamma'(|\mathbf{w}|)}{|\mathbf{w}|}S(|\mathbf{w}|)\right]d\mathbf{w}. \tag{48}$$

The integral has the same value for $j = 1$ and $j = 2$. We substitute (47) into (45) to obtain that

$$\left(i\rho\omega + \mu|\mathbf{k}|^2 - \frac{1/2\,\phi_0^2 M|\mathbf{k}|^2}{\beta_0 + i\omega}\right)\hat{\mathbf{u}} = 0. \tag{49}$$

For a nontrivial solution $\hat{\mathbf{u}}$ to exist, the dispersion relation

$$i\rho\omega + \mu|\mathbf{k}|^2 - \frac{1/2\,\phi_0^2 M|\mathbf{k}|^2}{\beta_0 + i\omega} = 0 \tag{50}$$

must hold. We introduce the notation $r = |\mathbf{k}|^2$ and note that the solutions to (50) are

$$\omega_\pm = \frac{i(\rho\beta_0 + \mu r) \pm \{Q(r)\}^{1/2}}{2\rho}, \tag{51}$$

where

$$Q(r) = -(\rho\beta_0 + \mu r)^2 - 4\rho(1/2\,\phi_0^2 M - \mu\beta_0)r, \tag{52}$$

or, alternatively (by completing the square),

$$Q(r) = -\mu^2\left\{r + \frac{\rho}{\mu^2}(\phi_0^2 M - \beta_0\mu)\right\}^2 + \frac{\rho^2}{\mu^2}\left\{(\phi_0^2 M - \beta_0\mu)^2 - \beta_0^2\mu^2\right\}. \tag{53}$$

Only if $Q(r) > 0$ for some $r > 0$ can the system have propagating plane wave solutions characteristic of an elastic material. We define

$$B = (\phi_0^2 M - \beta_0\mu)^2 - \beta_0^2\mu^2. \tag{54}$$

The sign of B determines whether there exist r for which $Q(r)$ is positive. The quantity M appears in each of (52)–(54), and so it is important to calculate it in some illuminating special cases. As we did earlier (see §3.2), we consider link formation that

occurs at a constant rate α_0 for $|\mathbf{v}| < r_0$, and not at all for $|\mathbf{v}| > r_0$. We also assume that each link has the stiffness function $S(|\mathbf{v}|) = K_0\,(1 - |\mathbf{v}|/d)$; i.e., the link acts as a linear spring with resting length d. Then M may be calculated from (48) to be

$$M = -\left(\frac{4\pi r_0^5}{15}\right) K_0 \left(\frac{\alpha_0}{\beta_0}\right)\left(1 - \frac{d}{r_0}\right). \tag{55}$$

We note that if $d < r_0$, then $M < 0$. This is the case in which links may form both under compression and extension. If $d > r_0$, then $M > 0$, but this corresponds to what we regard as the implausible situation of all links forming under compression. We note that if $\alpha(|\mathbf{v}|) = \alpha_0 e^{-|\mathbf{v}|^2/r_0^2}$, then M has the same qualitative character as in (55). Returning to (53) and (54), we see that $Q(r) \le 0$ if $B \le 0$, and the latter occurs if and only if $0 \le M \le 2\beta_0\mu\phi_0^{-2}$. If M falls in this range, then $\omega_\pm$ are purely imaginary for all r, and $\mathrm{Im}(\omega_\pm) \ge 0$, so that all wavenumbers are stable. If $M > 2\beta_0\mu\phi_0^{-2}$, then $B > 0$, but, as we see from (52), $Q(r) \le 0$ for all $r \ge 0$, and so again $\mathrm{Re}(\omega_\pm) = 0$ for all r. In this case, however, $\mathrm{Im}(\omega_-) < 0$ for all $r > 0$, and so every wavenumber is unstable. The origin of this instability can be understood by reference to (29), which gives the total viscosity of the fluid-link system in a shear flow. Equation (29) was derived under the same assumption about link formation that we make here, and under the assumption that each link behaves as a linear spring with zero resting length. If we set $d = 0$ in the expression for M above, then the total viscosity can be expressed in terms of M as $\mu - \frac{1}{2}M\phi_0^2/\beta_0$. The total viscosity is therefore *negative* if $M > 2\mu\beta_0\phi_0^{-2}$.

For the physically more plausible case that $M < 0$, we see that $B > 0$ and that there is a range (r_-, r_+) for which the quadratic function $Q(r)$ is positive. The endpoints of this interval are given by

$$r_\pm = \frac{\rho}{\mu^2}\left\{-(\phi_0^2 M - \beta_0\mu) \pm |\phi_0^2 M - \beta_0\mu|\left[1 - \beta_0^2\mu^2(\phi_0^2 M - \beta_0\mu)^{-2}\right]^{1/2}\right\}. \tag{56}$$

Since $(\phi_0^2 M - \beta_0\mu)^2 > \beta_0^2\mu^2$, $r_\pm$ have the same sign, and, since $\phi_0^2 M - \beta_0\mu < 0$, $r_\pm > 0$. So $Q(r)$ has the form shown in Fig. 3. For $r_- < r < r_+$, $\mathrm{Re}(\omega_\pm) \ne 0$ and $\mathrm{Im}(\omega_\pm) = \frac{1}{2}(\beta_0 + \mu r/\rho) > 0$, so these wavenumbers are stable. For $0 \le r \le r_-$ and $r_+ \le r$, $\mathrm{Re}(\omega_\pm) = 0$, $\mathrm{Im}(\omega_\pm) = (1/2\rho)\left\{(\rho\beta_0 + \mu r) \pm [-Q(r)]^{1/2}\right\}$, and $0 \le -Q(r) \le (\rho\beta_0 + \mu r)^2$, so all of these wavenumbers are stable as well. The point that we wish to emphasize is that, for $M < 0$, there is a range of wavenumbers for which propagating (and decaying) plane-wave solutions exist. Thus the fluid-link material has elastic as well as viscous characteristics. We also note that $r_- \to 0$ and $r_+ \to \infty$ as $M \to -\infty$, so that the range of wavenumbers for which elastic behavior occurs grows with increasing link stiffness (K_0), link-formation to link-breaking rate ratio (α_0/β_0), and activated platelet concentration (ϕ_0). The persistence of elastic behavior depends both on the fluid viscosity and the link-breaking rate.

3.4. Computational studies. While the linear stability analysis indicates that the fluid-link system has elastic characteristics, it is still not clear whether, in the full nonlinear equations that describe this system, the links can generate enough force to hold an aggregate together. After all, the platelets in the aggregate are assumed to move at the local fluid velocity, and if this velocity is not brought to zero by the action of the link forces, the aggregate will disintegrate. To address this question, we performed two-dimensional computational studies, which we now describe.

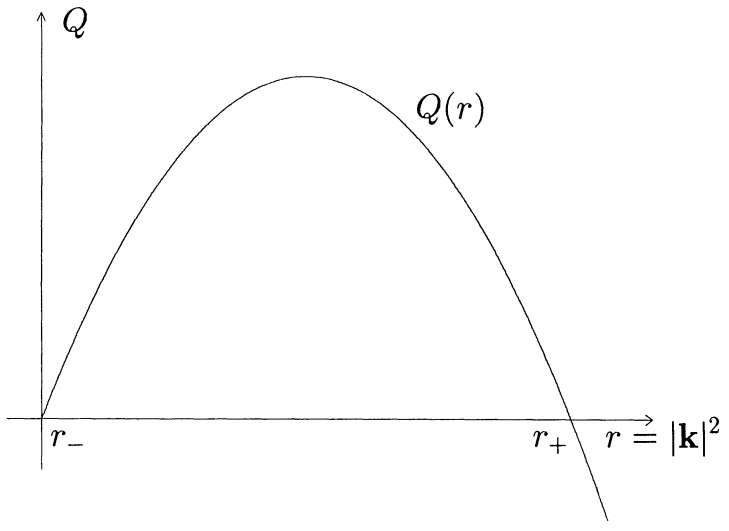

FIG. 3. *The discriminant $Q(r)$ in the solutions $\omega_\pm$ of the dispersion relation* (51) *in the case where $M < 0$. For $r \in (r_-, r_+)$, $\mathrm{Re}(\omega_\pm) \neq 0$. For the corresponding wavenumbers, there are propagating and decaying plane wave solutions to the linearized equations. The lower limit $r_- \approx 0$ because the fluid viscosity μ is small (see* (53)).

Under special, but reasonable, assumptions, the model as presented above can be recast into a form more suitable for computation. For the form of the model discussed thusfar, we would solve a transport equation (6) for P that involves two sets of spatial variables $\mathbf{x}$ and $\mathbf{v}$, as well as time. Then, to evaluate the cohesion-force density $\mathbf{f}^p$, we would have to perform an integration over $\mathbf{v}$ for *each* point $\mathbf{x}$. These are very computation-intensive tasks. If we assume that each link behaves as a linear spring with zero resting length ($S(|\mathbf{v}|) = K_0$), and that the rate at which links break $\beta(|\mathbf{v}|)$ is a constant β_0, then the model equations can be used to derive the following partial differential equation for the cohesion-stress tensor $\underline{\underline{\sigma}}^p$ (see Appendix C for the derivation):

$$\underline{\underline{\sigma}}^p{}_t + \mathbf{u} \cdot \nabla \underline{\underline{\sigma}}^p = \underline{\underline{\sigma}}^p \underline{\underline{\nabla \mathbf{u}}} + (\underline{\underline{\sigma}}^p \underline{\underline{\nabla \mathbf{u}}})^T + a_2 {\phi_a}^2 \underline{\underline{I}} - \beta_0 \underline{\underline{\sigma}}^p. \tag{57}$$

Here a_2 is a constant proportional to the second moment of $\alpha(|\mathbf{v}|)S(|\mathbf{v}|)$. The tensor $\underline{\underline{\nabla \mathbf{u}}}$ has elements $(\underline{\underline{\nabla \mathbf{u}}})_{ij} = \partial u_j / \partial x_i$. Note that all reference to the link vectors $\mathbf{v}$ disappears. Since $\underline{\underline{\sigma}}^p$ is a symmetric tensor, the above tensor equation amounts to solving three equations (in the two-dimensional case). Once we have $\underline{\underline{\sigma}}^p$, $\mathbf{f}^p$ is obtained by differentiation from the equation

$$\mathbf{f}^p = \nabla \cdot \underline{\underline{\sigma}}^p. \tag{58}$$

Solving (57) and then using (58) to obtain $\mathbf{f}^p$ is a much more efficient computational process than is determining P and then integrating to obtain $\mathbf{f}^p$.

It is also useful to have a measure for the intensity of aggregation within a region. In the model, aggregation manifests itself solely through the force-generating action of the links; so a reasonable measure of aggregation is the concentration of links at

each point $\mathbf{x}$. Thus the function

$$z(\mathbf{x},t) = \phi_a(\mathbf{x},t)^2 \int P(\mathbf{x},\mathbf{v},t)d\mathbf{v} \tag{59}$$

is used to measure aggregation. A transport equation for the scalar z can also be derived from the model's equations

$$z_t + \mathbf{u}\cdot\nabla z = a_0{\phi_a}^2 - \beta_0 z. \tag{60}$$

Here a_0 is proportional to the mean of $\alpha(|\mathbf{v}|)$.

We solved the initial value problem for the equations

$$\rho(\mathbf{u}_t + \mathbf{u}\cdot\nabla\mathbf{u}) = -\nabla p + \mu\Delta\mathbf{u} + \mathbf{f}^g + \mathbf{f}^p, \tag{61}$$

$$\nabla\cdot\mathbf{u} = 0, \tag{62}$$

$$\underline{\underline{\sigma}}^p{}_t + \mathbf{u}\cdot\nabla\underline{\underline{\sigma}}^p = \underline{\underline{\sigma}}^p\underline{\underline{\nabla\mathbf{u}}} + (\underline{\underline{\sigma}}^p\underline{\underline{\nabla\mathbf{u}}})^T, \tag{63}$$

$$\mathbf{f}^p = \nabla\cdot\underline{\underline{\sigma}}^p, \tag{64}$$

$$\frac{\partial\phi_a}{\partial t} + \mathbf{u}\cdot\nabla\phi_a = 0, \tag{65}$$

$$z_t + \mathbf{u}\cdot\nabla z = 0, \tag{66}$$

which describe the model in the case that there is no new platelet activation and no new formation or breaking of links. We note that in this case, (61)–(64) form a closed system, and we solve (65) and (66) just for visualization purposes. The equations are solved in a two-dimensional periodic domain. We determine the given force density $\mathbf{f}^g$, so that, in the absence of links, it would drive a steady and spatially periodic version of a stagnation point flow (this flow is shown in the first picture of Fig. 4, Column A). We specify an initial distribution of activated platelets ϕ_a with circular support centered at the stagnation point. Initial values of the link stress tensor were specified corresponding to this distribution of activated platelets and to an initially isotropic distribution of links $P(|\mathbf{v}|) = \alpha(|\mathbf{v}|)/\beta_0$. The function $\alpha(|\mathbf{v}|)$ is assumed to be that defined in (23). We consider the limit $\alpha_0 \to 0$ and $\beta_0 \to 0$ with α_0/β_0 fixed, so that there is an initial distribution of links but no link-formation or link-breaking terms in (63). The aggregation-intensity function z is initialized consistent with (59). In an experiment in which the link stiffness $K_0 = 0$ so that, in effect, the links are absent, the stagnation point flow stretches the initially circular distribution of platelets into a longer and longer ellipse. This is shown in Fig. 4. In this figure, the top row of pictures corresponds to the initial state and subsequent rows correspond to a succession of later times during the experiment. Column A depicts the velocity field, Column B shows contour lines of the aggregation-intensity function z, and Column C shows the locations of two sets of fluid marker points. The outermost aggregation-intensity contour is also shown in the pictures in Column A. For this experiment, the velocity field remains constant in time, and both the contours of z and the locations

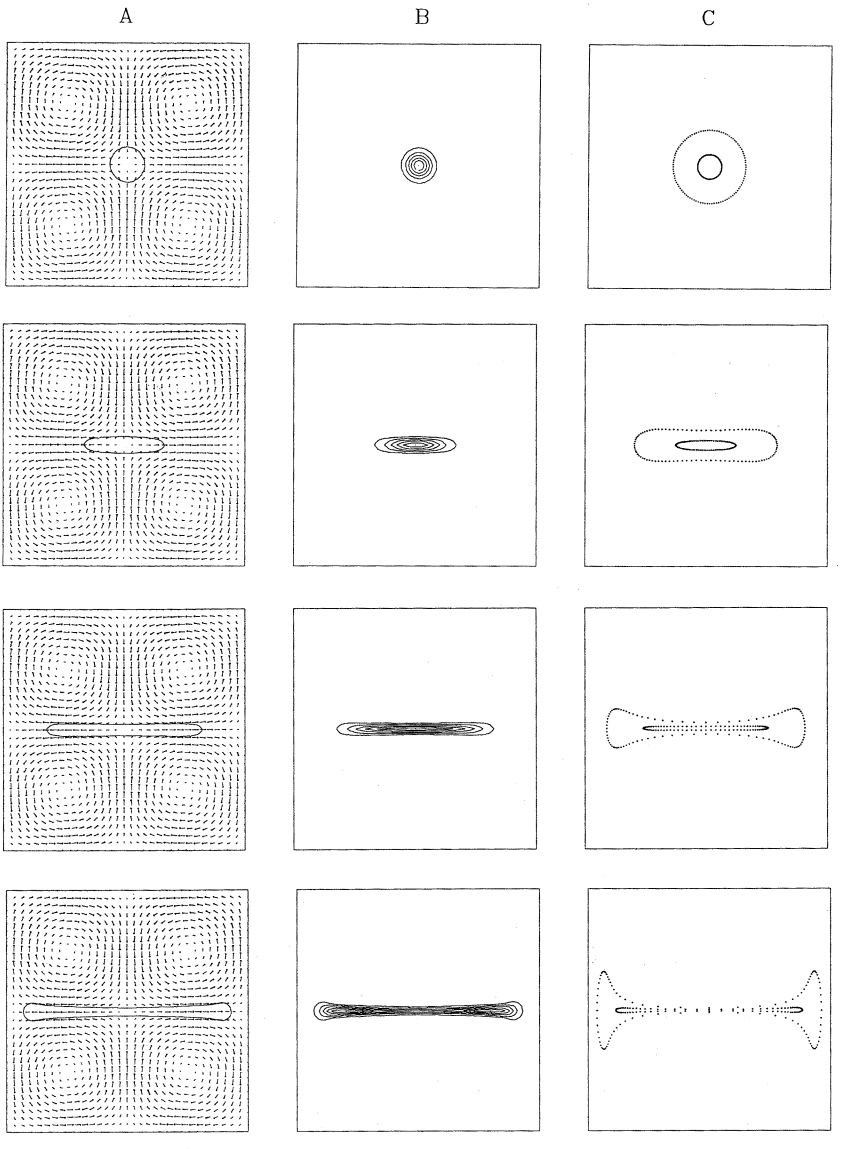

FIG. 4. *A sequence of snapshots from a computational experiment with the fluid-link system* (61)–(64). *Column* A *depicts the fluid velocity field* $\mathbf{u}$, *Column* B *shows contours of the aggregate-intensity function* z, *and Column* C *shows the locations of two sets of fluid marker points. The outermost contour of* z *is also shown in Column* A. *In this experiment, the link stiffness was zero, and the background stagnation-point flow induced progressive elongation of the initially circular aggregate and of the two sets of fluid markers.*

of the fluid markers show the effect of the resulting elongation. In another experiment in which links are present, the flow stretches the aggregate somewhat until the link forces are sufficient to balance the background flow (driven by $\mathbf{f}^g$), at which time the aggregate stabilizes. This experiment is depicted in Fig. 5. The effect of the links is most vividly illustrated by the motion of the two sets of fluid markers (see Fig. 5, Column C), one just on the edge of central core of the aggregate and the other substantially outside of it. The former deforms into an ellipse and then remains

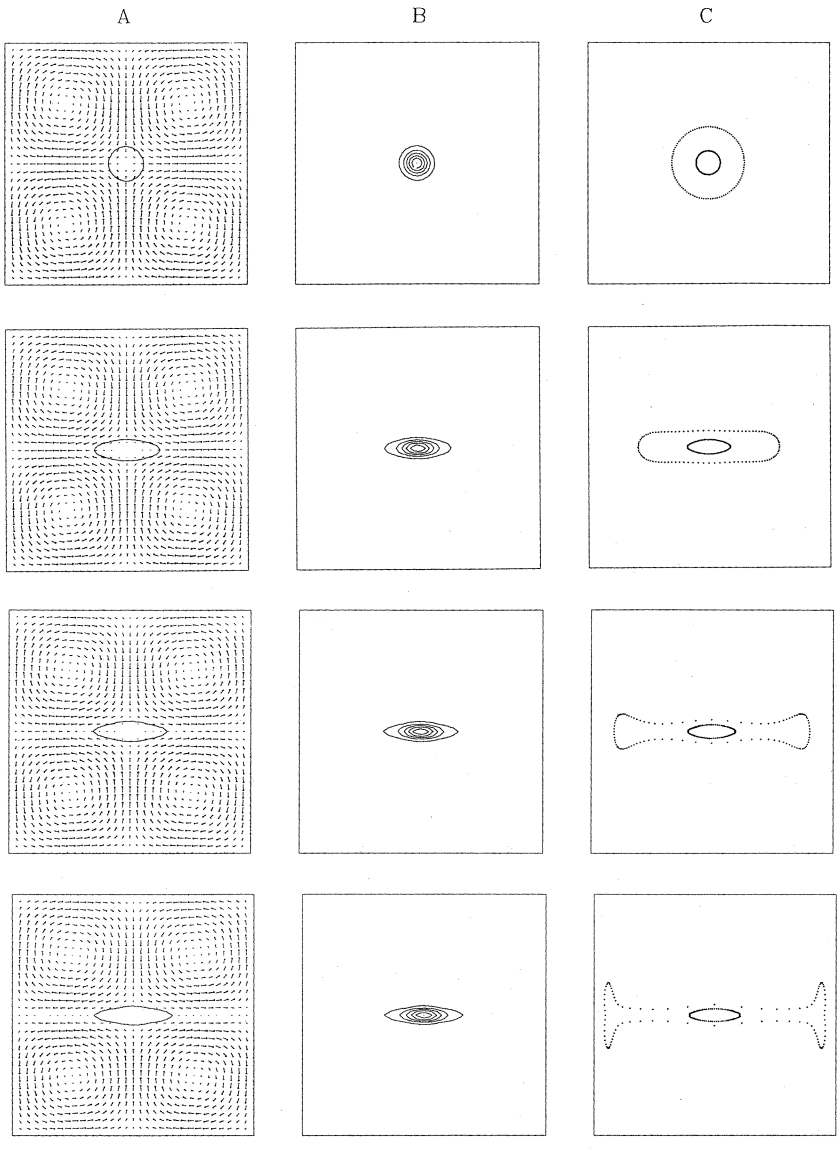

FIG. 5. *A sequence of snapshots similar to those shown in Fig. 4, but now from a computational experiment in which the link stiffness was nonzero. The initial state was the same as in the experiment depicted in Fig. 4. The aggregate was stretched somewhat by the background flow, but soon stabilized because of the action of the cohesive forces. The velocity within the aggregate dropped to zero by the last frame of Column A. As a consequence, the locations of the fluid markers within the aggregate also stabilized, while the the ring of fluid markers outside of the aggregate continued to deform. The material within the aggregate thus behaved as an elastic solid, while the material outside the aggregate behaved as a fluid.*

stationary, while the latter, little affected by the link forces, continues to stretch into a longer and longer ellipse under the influence of the background flow. We can also see from the last velocity field picture (the last picture of Column A), that the flow within the aggregate is essentially zero. The links do indeed imbue the fluid-link system with enough elasticity to withstand a substantial driving flow!

4. Conclusions. We have formulated continuum models of platelet aggregation and have examined their mechanical properties in the absence of activation chemistry. Cohesion between model platelets gives rise to extra pressure, and also to extra viscous and elastic stresses on the fluid in which the platelets are suspended. Sufficient elastic stress can be developed in the fluid-aggregate material to maintain the integrity and shape of an aggregate that is subject to a substantial elongational stress. Thus the presence of sufficient concentrations of activated platelets and interplatelet links within a portion of the suspending fluid can alter the behavior of the composite material from that of a viscous fluid to that of an elastic solid. In the full aggregation models there is thus the interesting possibility of a chemically-induced fluid-to-solid phase transition. This is a subject for future study.

Another subject for future study is the effect of allowing the link-breaking rate β to vary. Recall that, in this paper, we have assumed that $\beta = \beta_0$ is constant. It would be more interesting and probably more realistic for the breaking rate to be sensitive to the strain within an aggregate. This would be accomplished if, for example, we prescribed that $\beta(|\mathbf{v}|)$ be near zero for $|\mathbf{v}|$ small and that it increase rapidly with $|\mathbf{v}|$ when $|\mathbf{v}|$ crosses a threshold value. If this rule were incorporated into the full aggregation models, very interesting behavior might result. The central core of an aggregate in which the strain is not too large would behave as an elastic solid for long periods of time ($O(\beta^{-1})$). Greater shear stresses at the periphery of the aggregate would make the situation there more dynamic. Whether the aggregate would grow or shrink would be influenced by competition between new chemically-induced activation and link formation on the one hand, and shear-induced link breaking on the other hand. Furthermore, increased shear on the entire aggregate, due perhaps to temporal changes in the background flow, might strain even central regions of the aggregate sufficiently to induce rapid link breaking and the consequent shedding of portions of the aggregate. The special form of the model, which includes (57) and which was used in the computational studies reported in this paper, would not be applicable to studying this new situation. This is because (57) was derived under the assumption of constant breaking rate. It may be possible to derive a similar equation that is approximately true when β is variable. Alternatively, we may be able to develop efficient numerical schemes for solving the more basic form of the model, which involves the transport equation for P. Both of these possibilities are currently under investigation.

Appendix A. Derivation of the transport equation (6) for $(P\phi_a^2)$. Let $N(t)$ denote the total number of links between activated platelets in $\Omega_x(t)$ and activated platelets in $\Omega_y(t)$. The left side of (8) is the time derivative of $N(t)$, which we compute to obtain

$$\begin{aligned}\epsilon^6 \frac{d}{dt} N(t) = &\int_{\Omega_x(t)} \int_{\Omega_y(t)} \frac{d}{dt} \left\{ \phi_a(\mathbf{x},t)\phi_a(\mathbf{y},t)P(\mathbf{x},\epsilon^{-1}(\mathbf{y}-\mathbf{x}),t) \right\} d\mathbf{y}d\mathbf{x} \\ &+ \int_{\Omega_x(t)} \int_{\partial\Omega_y(t)} \phi_a(\mathbf{x},t)\phi_a(\mathbf{y},t)P(\mathbf{x},\epsilon^{-1}(\mathbf{y}-\mathbf{x}),t)\, \mathbf{u}(\mathbf{y},t)\cdot\mathbf{n}(\mathbf{y})\, da(\mathbf{y})d\mathbf{x} \\ &+ \int_{\Omega_y(t)} \int_{\partial\Omega_x(t)} \phi_a(\mathbf{x},t)\phi_a(\mathbf{y},t)P(\mathbf{x},\epsilon^{-1}(\mathbf{y}-\mathbf{x}),t)\, \mathbf{u}(\mathbf{x},t)\cdot\mathbf{n}(\mathbf{x})\, da(\mathbf{x})d\mathbf{y}.\end{aligned} \tag{A1}$$

Here d/dt denotes the total time derivative, $\mathbf{u}(\mathbf{y},t)$ ($\mathbf{u}(\mathbf{x},t)$) is the velocity of the point $\mathbf{y}(t) \in \partial\Omega_y(t)$ ($\mathbf{x}(t) \in \partial\Omega_x(t)$), and $\mathbf{n}(\mathbf{y})$ ($\mathbf{n}(\mathbf{x})$) is the unit outward normal to $\partial\Omega_y(t)$ ($\partial\Omega_x(t)$). We apply the divergence theorem to each of the surface integrals in

(A1) and use the incompressibility of the flow field $\mathbf{u}$ to obtain

$$\begin{aligned}\epsilon^6 \frac{d}{dt} N(t) = &\int_{\Omega_x(t)} \int_{\Omega_y(t)} \frac{d}{dt} \left\{ \phi_a(\mathbf{x},t)\phi_a(\mathbf{y},t) P(\mathbf{x}, \epsilon^{-1}(\mathbf{y}-\mathbf{x}), t) \right\} d\mathbf{y} d\mathbf{x} \\ &+ \int_{\Omega_x(t)} \int_{\Omega_y(t)} \mathbf{u}(\mathbf{y},t) \cdot \nabla_y \left\{ \phi_a(\mathbf{x},t)\phi_a(\mathbf{y},t) P(\mathbf{x}, \epsilon^{-1}(\mathbf{y}-\mathbf{x}), t) \right\} d\mathbf{y} d\mathbf{x} \\ &+ \int_{\Omega_x(t)} \int_{\Omega_y(t)} \mathbf{u}(\mathbf{x},t) \cdot \nabla_x \left\{ \phi_a(\mathbf{x},t)\phi_a(\mathbf{y},t) P(\mathbf{x}, \epsilon^{-1}(\mathbf{y}-\mathbf{x}), t) \right\} d\mathbf{y} d\mathbf{x}.\end{aligned} \tag{A2}$$

Let $\mathbf{v} = \epsilon^{-1}(\mathbf{y}-\mathbf{x})$ and, for each $\mathbf{x} \in \Omega_x(t)$, let $\Sigma_v(t) = \{\mathbf{v} : \mathbf{y} \equiv \mathbf{x} + \epsilon\mathbf{v} \in \Omega_y(t)\}$. Note that $\nabla_y = \epsilon^{-1}\nabla_v$ and $\nabla_x = -\epsilon^{-1}\nabla_v$. Substitute (A2) into (8) and make the change of variables from $\mathbf{y}-\mathbf{x}$ to $\mathbf{v}$ to obtain

$$\begin{aligned}&\int_{\Omega_x(t)} \int_{\Sigma_v(t)} \frac{d}{dt} \left\{ \phi_a(\mathbf{x},t)\phi_a(\mathbf{x}+\epsilon\mathbf{v},t) P(\mathbf{x},\mathbf{v},t) \right\} d\mathbf{v} d\mathbf{x} \\ &\quad + \int_{\Omega_x(t)} \int_{\Sigma_v(t)} \epsilon^{-1} \mathbf{u}(\mathbf{x}+\epsilon\mathbf{v},t) \cdot \nabla_v \left\{ \phi_a(\mathbf{x},t)\phi_a(\mathbf{x}+\epsilon\mathbf{v},t) P(\mathbf{x},\mathbf{v},t) \right\} d\mathbf{v} d\mathbf{x} \\ &\quad - \int_{\Omega_x(t)} \int_{\Sigma_v(t)} \epsilon^{-1} \mathbf{u}(\mathbf{x},t) \cdot \nabla_v \left\{ \phi_a(\mathbf{x},t)\phi_a(\mathbf{x}+\epsilon\mathbf{v},t) P(\mathbf{x},\mathbf{v},t) \right\} d\mathbf{v} d\mathbf{x} \\ &= \int_{\Omega_x(t)} \int_{\Sigma_v(t)} \alpha(|\mathbf{v}|)\, \phi_a(\mathbf{x},t)\phi_a(\mathbf{x}+\epsilon\mathbf{v},t)\, d\mathbf{v} d\mathbf{x} \\ &\quad - \int_{\Omega_x(t)} \int_{\Sigma_v(t)} \beta(|\mathbf{v}|)\, \phi_a(\mathbf{x},t)\phi_a(\mathbf{x}+\epsilon\mathbf{v},t) P(\mathbf{x},\mathbf{v},t)\, d\mathbf{v} d\mathbf{x}.\end{aligned} \tag{A3}$$

Now expand $\phi_a(\mathbf{x}+\epsilon\mathbf{v},t)$ and $\mathbf{u}(\mathbf{x}+\epsilon\mathbf{v},t)$ about the point $(\mathbf{x},t)$, insert these expansions into (A3), and retain only the zeroth-order terms to obtain

(A4)

$$\begin{aligned}&\int_{\Omega_x(t)} \int_{\Sigma_v(t)} \left[\frac{d}{dt} \left\{ \phi_a(\mathbf{x},t)^2 P(\mathbf{x},\mathbf{v},t) \right\} + (\mathbf{v}\cdot\nabla\mathbf{u}) \cdot \nabla_v \left\{ \phi_a(\mathbf{x},t)^2\, P(x,\mathbf{v},t)) \right\} \right] d\mathbf{v} d\mathbf{x} \\ &\qquad = \int_{\Omega_x(t)} \int_{\Sigma_v(t)} \phi_a(\mathbf{x},t)^2 \left\{ \alpha(|\mathbf{v}|) - \beta(|\mathbf{v}|) P(\mathbf{x},\mathbf{v},t) \right\} d\mathbf{v} d\mathbf{x}.\end{aligned}$$

We expand the total time derivative d/dt as $(\partial/\partial t + \mathbf{u}\cdot\nabla)$ and note that the integrands in (A4) must match because the regions $\Omega_x(t)$ and $\Sigma_x(t)$ are arbitrary. Equation (6) is the result.

Appendix B. Derivation of equation (7) for the cohesion-force density. We start with (9), make the substitution $\mathbf{F}(\epsilon^{-1}\mathbf{r}) = \epsilon^2 S(|\epsilon^{-1}\mathbf{r}|)\epsilon^{-1}\mathbf{r}$, and change variables $\mathbf{r} = \epsilon\mathbf{v}$ to obtain

$$\mathbf{f}^p(\mathbf{x},t) = \epsilon^{-1}\phi_a(\mathbf{x},t) \int P(\mathbf{x},\mathbf{v},t)\phi_a(\mathbf{x}+\epsilon\mathbf{v},t) S(|\mathbf{v}|)\mathbf{v} d\mathbf{v}. \tag{B1}$$

We next expand $\phi_a(\mathbf{x}+\epsilon\mathbf{v},t)$ about the point $(\mathbf{x},t)$ to obtain

$$\begin{aligned}\mathbf{f}^p(\mathbf{x},t) = &\epsilon^{-1}\phi_a(\mathbf{x},t)^2 \int P(\mathbf{x},\mathbf{v},t) S(|\mathbf{v}|)\mathbf{v} d\mathbf{v} \\ &+ \phi_a(\mathbf{x},t) \int P(\mathbf{x},\mathbf{v},t)(\mathbf{v}\cdot\nabla\phi_a(\mathbf{x},t)) S(|\mathbf{v}|)\mathbf{v} d\mathbf{v} + O(\epsilon).\end{aligned} \tag{B2}$$

We note that P is subject to the constraint

$$P(\mathbf{x}, -\mathbf{v}, t) = P(\mathbf{x} - \epsilon\mathbf{v}, \mathbf{v}, t) \tag{B3}$$

because both of these quantities describe the expected number of links that join a platelet at $\mathbf{x}$ and one at $\mathbf{x} - \epsilon\mathbf{v}$. Expanding the right-hand side of (B3) about the point $(\mathbf{x}, t)$ gives

$$P(\mathbf{x}, -\mathbf{v}, t) = P(\mathbf{x}, \mathbf{v}, t) - \epsilon\mathbf{v} \cdot \nabla_x P(\mathbf{x}, \mathbf{v}, t) + O(\epsilon^2). \tag{B4}$$

Define

$$I(\mathbf{x}, t) = \int P(\mathbf{x}, \mathbf{v}, t) S(|\mathbf{v}|)\mathbf{v} d\mathbf{v}. \tag{B5}$$

Make the change of variables $\mathbf{v} \to -\mathbf{v}$ in (B5) and use (B4) to conclude that

$$I(\mathbf{x}, t) = \epsilon \frac{1}{2} \int \mathbf{v} \cdot \nabla_x P(\mathbf{x}, \mathbf{v}, t) S(|\mathbf{v}|)\mathbf{v} d\mathbf{v} + O(\epsilon^2). \tag{B6}$$

Substitution of (B6) into the first term in (B2) yields (7) as the zeroth-order term.

Appendix C. Derivation of the transport equation for $\underline{\underline{\sigma}}^p$. Recall that

$$\underline{\underline{\sigma}}^p(\mathbf{x}, t) = \frac{1}{2}\phi_a(\mathbf{x}, t)^2 \int P(\mathbf{x}, \mathbf{v}, t) S(|\mathbf{v}|)\mathbf{v}\mathbf{v}^T d\mathbf{v}, \tag{C1}$$

and that, for all $\mathbf{x}$ and t, P decays rapidly as $|\mathbf{v}|$ grows, so that the validity of commuting differentiation with respect to $\mathbf{x}$ or t with integration with respect to $\mathbf{v}$ is not an issue. Let $d/dt = \partial/\partial t + \mathbf{u} \cdot \nabla$ denote the material derivative. Then we have that

$$\frac{d}{dt}(\underline{\underline{\sigma}}^p) = \frac{1}{2} \int \frac{d}{dt} \left\{\phi_a^2 P\right\} S(|\mathbf{v}|)\mathbf{v}\mathbf{v}^T d\mathbf{v}. \tag{C2}$$

Using (6) and assuming that $\beta(|\mathbf{v}|) = \beta_0$, we have that

$$\frac{d}{dt} \left\{\phi_a^2 P\right\} = -(\mathbf{v} \cdot \nabla\mathbf{u}) \cdot \nabla_v \left\{\phi_a^2 P\right\} + \alpha\phi_a^2 - \beta_0 \left\{\phi_a^2 P\right\}. \tag{C3}$$

Substituting (C3) into (C2) yields

$$\begin{aligned} \frac{d}{dt}(\underline{\underline{\sigma}}^p) = &-\frac{1}{2} \phi_a^2 \int (\mathbf{v} \cdot \nabla\mathbf{u}) \cdot \nabla_v(P) S(|\mathbf{v}|)\mathbf{v}\mathbf{v}^T d\mathbf{v} \\ &+ a_2\phi_a^2 \underline{\underline{I}} - \beta_0 \underline{\underline{\sigma}}^p, \end{aligned} \tag{C4}$$

where $a_2 = \frac{1}{6} \int \alpha(|\mathbf{v}|) S(|\mathbf{v}|) |\mathbf{v}|^2 d\mathbf{v}$ and $\underline{\underline{I}}$ is the identity matrix. Consider that the klth element of the integral in (C4) is

$$\int (\mathbf{v} \cdot \nabla\mathbf{u}) \cdot \nabla_v(P) S(|\mathbf{v}|) v_k v_l d\mathbf{v} = \int \Sigma_i \Sigma_j v_j \frac{\partial u_i}{\partial x_j} \frac{\partial P}{\partial v_i} S(|\mathbf{v}|) v_k v_l d\mathbf{v}, \tag{C5}$$

which, upon integration by parts with respect to v_i, becomes

$$\begin{aligned} = &- \int \left[\Sigma_i \Sigma_j P \left(\frac{\partial v_j}{\partial v_i}\right) \left(\frac{\partial u_i}{\partial x_j}\right) S(|\mathbf{v}|) v_k v_l\right] d\mathbf{v} \\ &- \int \left[\Sigma_i \Sigma_j P v_j \left(\frac{\partial u_i}{\partial x_j}\right) S'(|\mathbf{v}|) \frac{\partial |\mathbf{v}|}{\partial v_i} v_k v_l\right] d\mathbf{v} \\ &- \int \left[\Sigma_i \Sigma_j P v_j \left(\frac{\partial u_i}{\partial x_j}\right) S(|\mathbf{v}|) \frac{\partial}{\partial v_i}(v_k v_l)\right] d\mathbf{v}. \end{aligned}$$

The first term vanishes because $\nabla \cdot \mathbf{u} = 0$, and the second term vanishes because we have assumed that $S(|\mathbf{v}|) = K_0 = \text{constant}$. The third term can be rewritten after a little algebra as

$$-\int \left[\Sigma_j v_k v_j \frac{\partial u_l}{\partial x_j}\right] PS d\mathbf{v} - \int \left[\Sigma_j v_l v_j \frac{\partial u_k}{\partial x_j}\right] PS d\mathbf{v},$$

which is the klth element of

$$-\int \left(\mathbf{v}\mathbf{v}^T \underline{\underline{\nabla \mathbf{u}}}\right) PS d\mathbf{v} - \int \left(\mathbf{v}\mathbf{v}^T \underline{\underline{\nabla \mathbf{u}}}\right)^T PS d\mathbf{v}.$$

Substitution of this expression into (C4) yields the desired transport equation for $\underline{\underline{\sigma}}^p$. We note that, without the assumptions that $\beta(|\mathbf{v}|) = \beta_0$ and $S(|\mathbf{v}|) = K_0$, the transport equation for $\underline{\underline{\sigma}}^p$ would involve higher moments of PS, and the system would not close.

Acknowledgments. The author thanks C. S. Peskin, R. Caflisch, and J. Keener for helpful discussions and advice.

REFERENCES

[1] G. A. Adams and I. A. Feuerstein, *Platelet adhesion and release: Interfacial concentration of released materials*, Amer. J. Physiol., 240 (1981), pp. H99–H108.

[2] ———, *Maximal fluid concentrations of materials released from platelets at a surface*, Amer. J. Physiol., 244 (1983), pp. H109–H114.

[3] L. Badimon, J. J. Badimon, V. T. Turitto, S. Vallabhajosula, and V. Fuster, *Platelet thrombus formation on collagen type* I, Circulation, 78 (1988), pp. 1431–1442.

[4] G. K. Batchelor, *An Introduction to Fluid Dynamics*, Cambridge University Press, Cambridge, England, 1967.

[5] J. Caen, S. Cronberg, and P. Kubisz, *Platelets: Physiology and Pathology*, Stratton Intercontinental Medical Book, New York, 1977.

[6] T. C. Detwiler and E. M. Huang, *Interactions of platelet activating factor pathways: Interrelationships of aggregation and secretion*, in Platelet Responses and Metabolism, Vol. I: Responses, H. Holmsen, ed., CRC Press, Boca Raton, FL, 1986, pp. 235–249.

[7] L. A. Fitzgerald and D. R. Phillips, *Platelet membrane glycoproteins*, in Hemostasis and Thrombosis, R. W. Colman, J. Hirsh, V. J. Marder, and E. W. Salzman, eds., J. B. Lippincott, Philadelphia, PA, 1987, pp. 572–593.

[8] A. L. Fogelson, *A mathematical model and numerical method for studying platelet adhesion and aggregation during blood clotting*, J. Comput. Phys., 56 (1984), pp. 111–134.

[9] J. S. Forrester, F. Litvack, W. Grundfest, and A. Hickey, *A perspective of coronary disease seen through the arteries of living man*, Circulation, 75 (1987), pp. 6–14.

[10] V. Fuster, L. Badimon, M. Cohen, J. A. Ambrose, J. J. Badimon, and J. Cheesbro, *Insights into the pathogenesis of acute ischemic syndromes*, Circulation, 77 (1988), pp. 15–22.

[11] A. R. L. Gear, *In vitro platelet responses: Aggregation*, in Platelet Responses and Metabolism, Vol. I: Responses, H. Holmsen, ed., CRC Press, Boca Raton, FL, 1986, pp. 97–114.

[12] H. L. Goldsmith and T. Karino, *Microscopic considerations: The motions of individual particles*, in Annals of the New York Academy of Sciences, Vol. 283, L. Vroman and E. F. Leonard, eds., New York, 1977, pp. 241–255.

[13] E. F. Grabowski, L. I. Friedman, and E. F. Leonard, *Effects of shear rate on the diffusion and adhesion of blood platelets to a foreign surface*, Indust. Engrg. Chem. Fund., 11 (1972), pp. 224–232.

[14] E. F. Grabowski, J. T. Franta, and P. Didisheim, *Platelet aggregation in flowing blood in vitro* II. *Dependence of aggregate growth rate on* ADP *concentration and shear rate*, Microvascular Res., 16 (1978), pp. 183–195.

[15] H. Holmsen, L. Salganicoff, and M. H. Fukami, *Platelet behavior and biochemistry*, in Haemostasis: Biochemistry, Physiology, and Pathology, Ogston and Bennett, eds., John Wiley, New York, 1977.

[16] J. A. HUBBEL AND L. V. MCINTIRE, *Platelet active concentration profiles near growing thrombi*, Biophys. J., 50 (1986), pp. 937–945.

[17] T. KARINO AND H. L GOLDSMITH, *Aggregation of human platelets in an annular vortex distal to a tubular expansion*, Microvascular Res., 17 (1979), pp. 217–237.

[18] B. LAGES, *In vitro platelet responses: Dense granule secretion*, in Platelet Responses and Metabolism, Vol. I: Responses, H. Holmsen, ed., CRC Press, Boca Raton, FL, 1986, pp. 115–143.

[19] G. MARGUERIE, M. H. GINSBERG, AND E. F. PLOW, *Glycoproteins: The fibrinogen receptor*, in Platelet Responses and Metabolism, Vol. III: Response-Metabolism Relationships, H. Holmsen, ed., CRC Press, Boca Raton, FL, 1986, pp. 285–296.

[20] V. T. TURITTO, A. M. BENIS, AND E. F. LEONARD, *Platelet diffusion in flowing blood*, Indust. Engrg. Chem. Fund., 11 (1972), pp. 216–223.

[21] V. T. TURITTO AND H. R. BAUMGARTNER, *Platelet interaction with subendothelium in a perfusion system*, Microvascular Res., 9 (1975), pp. 335–344.

[22] V. T. TURITTO, R. MUGGLI, AND H. R. BAUMGARTNER, *Physical factors influencing platelet deposition on subendothelium: Importance of blood shear rate*, in Annals of the New York Academy of Sciences, 283, L. Vroman and E. F. Leonard, eds., New York, 1977, pp. 284–292.

[23] V. T. TURITTO AND H. R. BAUMGARTNER, *Platelet interaction with subendothelium in flowing rabbit blood: Effect of blood shear rate*, Microvascular Res., 17 (1979), pp. 38–54.

[24] V. T. TURITTO, H. J. WEISS, AND H. R. BAUMGARTNER, *The effect of shear rate on platelet interaction with subendothelium exposed to citrated human blood*, Microvascular Res., 19 (1980), pp. 352–365.

[25] V. T. TURITTO AND H. R. BAUMGARTNER, *Platelet-surface interactions*, in Hemostasis and Thrombosis, R. W. Colman, J. Hirsh, V. J. Marder, and E. W. Salzman, eds., J. B. Lippincott, Philadelphia, PA, 1987, pp. 555–571 .

[26] N. L. WANG AND K. H. KELLER, *Augmented transport of extracellular solutes in concentrated erythrocyte suspensions in couette flow*, J. Coll. Interface Sci., 103 (1985), pp. 210–225.

[27] H. J. WEISS, *Platelet physiology and abnormalities of platelet function (Part 1)*, New England J. Med., 293 (1975), pp. 531–541.

[28] J. G. WHITE, *Anatomy and structural organization of the platelet*, in Hemostasis and Thrombosis, R. W. Colman, J. Hirsh, V. J. Marder, and E. W. Salzman, eds., J. B. Lippincott, Philadelphia, PA, 1987, pp. 537–554.